Europe PMC Funders Group
Author Manuscript
Nat Methods. Author manuscript; available in PMC 2019 March 01.

Published in final edited form as:
Nat Methods. 2018 September ; 15(9): 748. doi:10.1038/s41592-018-0118-8.

Genetically engineered cerebral organoids model brain tumor formation

Shan Bian[1], **Marko Repic**[1,‡], **Zhenming Guo**[1,2], **Anoop Kavirayani**[3], **Thomas Burkard**[1,4], **Joshua A. Bagley**[1], **Christian Krauditsch**[1], **Jürgen A. Knoblich**[1,*]

[1]Institute of Molecular Biotechnology of the Austrian Academy of Sciences (IMBA), Vienna, Austria

[2]Bio-X Institute, Shanghai Jiao Tong University, Shanghai, China

[3]Vienna Biocenter Core Facilities (VBCF), Vienna, Austria

[4]Research Institute of Molecular Pathology (IMP), Vienna, Austria

Abstract

Brain tumors are among the most lethal and devastating cancers. Their study is limited by genetic heterogeneity and the incompleteness of available laboratory models. Three-dimensional organoid culture models offer innovative possibilities for the modeling of human disease. Here we establish a 3D in vitro model called a neoplastic cerebral organoid (neoCOR), in which we recapitulate brain tumorigenesis by introducing oncogenic mutations in cerebral organoids via transposon- and CRISPR–Cas9-mediated mutagenesis. By screening clinically relevant mutations identified in cancer genome projects, we defined mutation combinations that result in glioblastoma-like and central nervous system primitive neuroectodermal tumor (CNS-PNET)-like neoplasms. We demonstrate that neoCORs are suitable for use in investigations of aspects of tumor biology such as invasiveness, and for evaluation of drug effects in the context of specific DNA aberrations. NeoCORs will provide a valuable complement to the current basic and preclinical models used to study brain tumor biology.

[*]Correspondence (lead contact): juergen.knoblich@imba.oeaw.ac.at.
[‡]Present address: MC Toxicology Consulting, Vienna, Austria

Reporting Summary
Further information on experimental design is available in the Nature Research Reporting Summary linked to this article.

Data Availability
RNA-seq data are available in GEO under accession numbers GSE101577and GSE110611. The data that support the findings of this study are available from the corresponding author upon request. Source data for Figs. 2, 3, and 6 and Supplementary Figs. 1, 2, and 8 are available online.

Author Contributions
S.B. and J.A.K conceived the project and experimental design and wrote the manuscript. S.B. performed experiments and analysed data. M.R, Z.G., and C.K. performed experiments. A.K contributed the histopathology data. T.R.B performed bioinformatics analysis of RNA-seq data. J.A.B contributed in RNA-seq analysis and quantification of immunostained tissues. J.A.K directed and supervised the project.

Competing Financial Interests
S.B. and J.A.K. have filed a patent application for using this method in future disease modelling and pre-clinical investigation.

Europe PMC Funders Author Manuscripts
Europe PMC Funders Author Manuscripts

Europe PMC Funders Author Manuscripts

Europe PMC Funders Author Manuscripts

Introduction

Malignant brain tumors are among the most devastating cancers, with almost negligible survival rates1 that have not improved in decades, despite numerous studies of these tumors in many experimental model systems. Thus there is a need for new experimental model systems in which to study human brain tumors.

Among the currently available models, genetically engineered mouse models (GEMMs) are broadly used for both biological and preclinical investigations. GEMMs relatively accurately mimic the pathophysiological features of human brain tumors, but their application is limited by the genetic, morphological, and physiological differences between human and rodent brains2. GEMMs are also relatively expensive and time consuming to establish, which makes them suboptimal as a screening system for tumorigenic drivers from among the numerous candidates identified by brain cancer sequencing projects3–5. Patient-derived xenografts represent, to a large extent, the heterogeneity of human brain tumors, but they are not suitable for studies of tumor initiation. Furthermore, xenografts derived from biopsies take time to establish, and their use is financially infeasible for drug testing6. 2D cultures of human brain cancer cell lines and cancer stem cells have served as surrogate models for brain tumors but do not recapitulate the 3D tumor environment7,8. Tumor sphere models generated from either tumor cell lines or cancer stem cells mimic a 3D structure but lack organ-like histology and the interaction between tumor and normal tissues9,10.

The recent development of in vitro organoid culture has opened new avenues for disease modeling directly in human tissues. By recapitulating either organ regeneration from adult stem cells11 or organ development from pluripotent stem cells12, organoids can accurately represent organ histology and physiology13,14. Organoids have been used to model various human diseases15, including cancer16. Human cerebral organoids recapitulate human brain development *in vitro*, and have been used to model human neurodevelopmental disorders17–20. Thus far, no in vitro 3D organoid models have been developed that could be used to study human brain tumor initiation, progression, and treatment.

Here we report the development of 3D organoid models for the study of human brain tumor initiation, progression, and response to perturbation. We applied genome-editing techniques to introduce tumorigenic mutations into human cerebral organoids. These models allowed us to test the tumorigenic capability of gain- and loss-of-function mutations, singly or in combination, in a systematic manner. We show that mutations found in cancer patients resulted, in our model system, in xeno-transplantable tumors that could be classified as CNS-PNET or glioblastoma (GBM). The neoCOR model is a valuable tool that can be used to study fundamental brain tumor biology and test potential drugs in a personalized setting.

Results

Clonal mutagenesis in cerebral organoids induces tumor overgrowth

A recent reclassification of brain cancer subtypes includes DNA aberrations as a defining feature21, highlighting the need for genetically defined human brain cancer models. Brain

Europe PMC Funders Author Manuscripts

Europe PMC Funders Author Manuscripts

tumors are characterized by a variety of DNA aberrations that cause oncogene overexpression and/or loss of tumor-suppressor gene function3–5.

To recapitulate tumorigenic events in cerebral organoids, we combined Sleeping Beauty (SB) transposon-mediated gene insertion for oncogene amplification with CRISPR–Cas9-based mutagenesis of tumor-suppressor genes. We introduced combinations of plasmids into cerebral organoids by electroporation before embedding the organoids in Matrigel (Supplementary Fig. 1a). The plasmids used encode (1) the SB transposase for integration of inverted repeat (IR)-flanked expression elements into the genome, (2) GFP flanked by SB IRs for cell tracing, (3) any oncogene flanked by IRs for oncogene overexpression, and (4) plasmids expressing the Cas9 nuclease together with guide RNAs for mutagenesis of tumor-suppressor genes in cerebral organoids. This strategy gave us the flexibility to introduce any combination of gain- and/or loss-of-function tumorigenic genes.

At the end of the neural induction stage of our cerebral-organoid-development protocol17 (Fig. 1a), neural stem and progenitor cells (NS/PCs), which are believed to be cells of origin for many different brain tumor subtypes22–29, are expanding on the surface of embryoid bodies (EBs). Immunostaining of both sectioned EBs and adherent cultured EBs 1 d after nucleofection of pCAG-GFP showed that 100% of GFP^+ cells were $SOX1^+$, $CDH2^+$ (N-cadherin$^+$), and NES^+ NS/PCs (Fig. 1b). None of the GFP^+ cells were brachyury$^+$ (BRA^+) or $FOXF1^+$mesodermal cells, or $SOX17^+$ or $PECAM1^+$ ($CD31^+$) endodermal cells (Fig. 1b and Supplementary Fig. 1b–d). Thus, the electroporated plasmids were delivered exclusively into NS/PCs.

We tested whether tumorous overgrowth can be induced in cerebral organoids. We introduced into the organoids 18 single gene mutations or amplifications, as well as 15 of the most common clinically relevant combinations observed in brain tumors such as GBM3, pediatric CNS-PNET30, atypical teratoid/rhabdoid tumor31, and medulloblastoma5 (Supplementary Table 1). As most electroporated cells carried the CAG-GFP insertion, we used GFP intensity to quantify the proliferation of cells carrying gene aberrations. One day after electroporation, EBs from all groups contained similar amounts of GFP^+ cells (Fig. 2a,b). One month later, however, we observed striking overgrowth of GFP^+ cells in organoids carrying the *MYC* amplification (MYC^{OE}, where OE indicates overexpression) and in organoids with $CDKN2A^{-/-}/CDKN2B^{-/-}/EGFR^{OE}/EGFRvIII^{OE}$, $NF1^{-/-}/PTEN^{-/-}/TP53^{-/-}$ ($p53^{-/-}$), and $EGFRvIII^{OE}/CDKN2A^{-/-}/PTEN^{-/-}$ genotypes (Fig. 2a,c), where *EGFRvIII*denotes epidermal growth factor receptor variant III, a deletion variant of *EGFR1*/*ERBB1*/*HER1*. As these combinations of gene aberrations are commonly found in GBM, we refer to them as GBM-1, GBM-2, and GBM-3, respectively.

To confirm that the genome-editing techniques actually altered the genome in tumor cells, we analyzed the expression of oncogenes and/or sequencing CRISPR-targeting regions. We observed that tumor cells carried the expected gene mutations/amplifications (Supplementary Fig. 2a–d). Thus, cerebral organoids can be used as a platform to test the tumorigenic capacity of different gene aberrations.

Europe PMC Funders Author Manuscripts

Europe PMC Funders Author Manuscripts

MYC^{OE} and GBM-like neoCORs have distinct transcriptional profiles

To test whether brain-tumor-like organoids resemble distinct brain tumor subtypes, we carried out transcriptome analysis of GFP$^+$ cells isolated by FACS. Principal component analysis of the top 500 variable genes between different groups identified three distinct clusters. Cluster 1 included all control (CTRL) organoids, which harbored only CAG-GFP and a control guide RNA targeting dTomato (Fig. 3a). Cluster 2 included the organoids carrying the *MYC*^{OE} construct, and cluster 3 contained the organoids carrying genetic aberrations found in GBM (GBM-1, GBM-2, and GBM-3). On the basis of these clusters, we identified genes that were differentially expressed (DESeq, adjusted *P*value < 0.05) between cluster 2 or cluster 3 and CTRL. As expected, the Venn diagram hypergeometric test showed that the majority of genes that were deregulated in the *MYC*^{OE} group (cluster 2) were distinct from those deregulated in the GBM groups (cluster 3) (Supplementary Fig. 3a). Further KEGG pathway analysis of genes with differential expression (DESeq, adjusted *P* value < 0.05) between cluster 2 and cluster 3 indicated upregulation of metabolic pathway and cell-cycle genes in the tumor cells from cluster 2 neoCORs, as well as the Hippo, WNT, TGFβ, and TP53 signaling pathways, which are known to be connected to MYC32–34 (Supplementary Fig. 3b). In addition, the *MYC*^{OE} group showed upregulation of an epithelial differentiation signature, suggestive of a CNS-PNET-like neoplasm of neuroepithelial cellular origin. KEGG pathway analysis also confirmed a glioma signature in cluster 3 neoCORs, and showed upregulation of the PI3K–AKT, RAP1, ERBB, HIF1A, NF-κB, and estrogen signaling pathways, relevant for GBM35–39 (Supplementary Fig. 3b).

To test the similarity between the tumor cells from neoCORs and primary tumors, we examined the transcriptome data from neoCORs for genes known to be differentially expressed between CNS-PNET and GBM tumors30. Hierarchical clustering revealed that neoCORs from the *MYC*^{OE} group showed a strong CNS-PNET signature, whereas organoids from cluster 3 showed upregulation of GBM genes (Fig. 3b). These data suggest that we developed two distinct types of tumor overgrowth in human cerebral organoids, depending on the genetic aberrations induced: CNS-PNET-like and GBM-like neoplastic growths.

MYC^{OE} and GBM-like neoCORs have different cellular identities

In humans, CNS-PNETs are embryonic neuroepithelial neoplasms characterized by sheets of primitive neuroepithelial cells and frequent rosette formations40. These undifferentiated cells feature SOX2 expression and high CD99 expression41. GBMs, in contrast, are high-grade astrocytic neoplasms with a more diverse morphology featuring glial cell predominance. The glial markers GFAP and S100β, as well as the proliferative marker Ki67, are diagnostic for GBM.

We analyzed the expression of CNS-PNET and GBM markers in *MYC*^{OE} and GBM neoCORs 4 months after nucleofection. In CTRL organoids, most GFP$^+$ cells were HuC/D$^+$ neurons (Fig. 3c,d and Supplementary Fig. 4a), whereas only a small portion of GFP$^+$ cells were positive for SOX2 (Fig. 3c,e and Supplementary Fig. 4b) and Ki67 (Fig. 3c,f and Supplementary Fig. 4c) or the glial markers S100β (Fig. 3c,g and Supplementary Fig. 4d) and GFAP (Fig. 3c,h and Supplementary Fig. 4e). GFP$^+$ cells located in the ventricular zone

Europe PMC Funders Author Manuscripts

Europe PMC Funders Author Manuscripts

of cortical regions expressed SOX2 and Ki67, whereas GFP^+HuC/D^+ neurons were located in the basal cortical regions (Fig. 3c and Supplementary Fig. 4a–f).

In contrast, the MYC^{OE} organoids contained few GFP^+ cells that were HuC/D^+ (Fig. 3c,d and Supplementary Fig. 4a) or that expressed the glial marker S100β (Fig. 3c,g and Supplementary Fig. 4d) or GFAP (Fig. 3c,h and Supplementary Fig. 4e). Instead, most GFP^+ cells were $SOX2^+$ (Fig. 3c,e and Supplementary Fig. 4b), and nearly 50% expressed Ki67 (Fig. 3c,f and Supplementary Fig. 4c). In addition, most GFP^+ MYC^{OE} cells expressed high levels of CD99 antigen (Fig. 3c,i and Supplementary Fig. 4f), which further confirmed their CNS-PNET-like cellular identities. GFP^+ cells formed large sheets of cells and rosette structures (Fig. 3c and Supplementary Fig. 4a–f).

In the GBM-like groups, GFP^+ regions were positive for S100β (Fig. 3c,g, and Supplementary Figs. 4d and 5) and GFAP (Fig. 3c,h and Supplementary Figs. 4e and 5), indicating their glial identity, and contained only a few HuC/D^+ neurons (Fig. 3c,d, and Supplementary Figs. 4a and 5). Compared with CTRL organoids, they also contained more $SOX2^+$ (Fig. 3c,e and Supplementary Figs. 4b and 5) and $Ki67^+$ (Fig. 3c,f and Supplementary Figs. 4c and 5) cells, which are often observed in the central core of GBM tumors42. In addition, GFP^+ regions in GBM-relevant groups showed elevated CD99 levels compared with those in CTRL samples (Fig. 3c,i and Supplementary Figs. 4f and 5), a feature also reported for GBM tissues43. Tumor regions in the GBM-like organoids showed a disorganized architecture (Fig. 3c and Supplementary Figs. 4a–f and 5).

We also examined 1-month-old CTRL organoids and neoCORs, which had cellular identities and histological features similar to those of 4-month-old organoids (Supplementary Figs. 6a–e and 7a–e). Thus, neoCORs induced by distinct genetic aberrations recapitulate the cellular identities and partial histomorphological features of CNS-PNET or GBM tumors.

NeoCORs retain viability and expand after renal subcapsular engrafting

A capacity for self-renewal and immortality are two hallmarks of cancer cells. To examine whether neoCORs exhibited these features in vivo, we implanted them into the renal subcapsular space in immunodeficient mice (Supplementary Fig. 8a). Four out of five control organoids were resorbed within 6 weeks, and the remaining organoid was reduced to only a tiny cluster of cells (Fig. 4a) with diminished cellularity and architectural detail (Fig. 4b). In contrast, 17 out of 20 neoCORs were retained, and several expanded beyond the renal capsule by the end of the experimental period (Fig. 4a and Supplementary Fig. 8b). Immunohistochemical analysis revealed many neuroepithelial areas in organoids of the MYC^{OE} group positive for the NS/PC marker SOX1 (Fig. 4c) and cell-cycle marker Ki67 (Fig. 4d), but very few cells positive for the glial marker GFAP (Fig. 4e) or the neuronal marker MAP2 (Supplementary Fig. 8c), indicating their primitive, poorly differentiated state. Transplanted organoids from the MYC^{OE} group proliferated massively (Fig. 4a and Supplementary Fig. 8b). They formed cell sheets and rosettes, similar to CNS-PNET (Fig. 4b and Supplementary Fig. 8d–f). GBM groups instead showed high expression of the glial marker GFAP, NS/PC marker SOX1, and Ki67 (Fig. 4c–e). GBM-1 and GBM-3 organoids displayed a glial neoplasm-like expansion (Fig. 4b), whereas GBM-2 organoids showed glial neoplasm-like proliferation with additional cells of mature neuronal appearance reminiscent

of glioneuronal tumors (Fig. 4b). Thus, neoCORs can engraft and expand in vivo and maintain their subtype identity after renal transplantation into nude mice.

Use of GBM-like neoCORs to study interactions between tumor and normal tissue

Compared with other in vitro brain tumor models, a distinct feature of the neoCOR model is that tumors are initiated by the introduction of genetic aberrations into a very small portion of cells in the cerebral organoid. This not only mimics in vivo human tumor initiation, but also results in a mixed structure that contains both tumor and normal tissues. This allowed us to use neoCORs to study important properties such as invasiveness.

GBMs are known to display extensive infiltration of adjacent brain parenchyma, accompanied by an epithelial–mesenchymal transition that confers invasive capabilities to tumor cells44,45. To assess whether neoCORs can be used to study this process, we evaluated the interface between tumor and normal cells in GBM-like neoCORs. We observed GFP^+ tumor cells in normal regions (Fig. 5a–c). We also observed small foci of tumor cells that breached the renal capsule in the renal xenografts of GBM-group neoCORs (Fig. 5d).

We compared the expression levels of invasion-related genes in tumor cells from 4-month-old neoCORs of all three GBM groups and normal cells from same-age CTRL organoids, using RNA-seq analysis of FACS-sorted cells. Hierarchical clustering of samples based on reported GBM invasiveness-relevant genes46, including genes that encode transcription factors related to epithelial–mesenchymal transition (*TGFB*, *TGFB1I1*, *STAT3*, *SNAI2*, *ZEB1*, *ZEB2*), migration-related receptor (*CXCR4*), extracellular matrix molecules (*ITGA5*), and proteases (*PLAU*, *CTSB*, *ADAM10*, *ADAM17*, *MMP2*, *MMP14*), showed that tumor cells from all GBM neoCORs clustered together and had higher expression levels of invasiveness-relevant genes compared with those in normal cells from CTRL organoids and tumor cells from the MYC^{OE} group (Fig. 5e). In addition, tumor cells from all GBM groups exhibited downregulation of many genes involved in the inhibition of tumor invasion compared with expression in normal cells in CTRL organoids, such as genes encoding tissue inhibitors of matrix metalloproteinases (*TIMP2*, *TIMP3*) and tight junction components (*CLDN1*, *CLDN2*, *CLDN3*, *OCLN*)46 (Fig. 5e). We further clustered tumor cells from different GBM groups into individual groups on the basis of expression levels of various invasiveness-related genes. Most invasion-related genes were downregulated in MYC^{OE} neoCORs compared with their expression in the GBM groups (Fig. 5e), which correlates with the lower infiltration tendency of embryonic neoplasms compared with that of astrocytic neoplasms40.

Immunostaining of organoids for the mesenchymal marker vimentin (VIM), urokinase (PLAU), and matrix metalloproteinase 2 (MMP2) confirmed that tumor cells in GBM neoCORs expressed these invasiveness genes at higher levels compared with those in the surrounding normal tissues (Fig. 5f).

NeoCORs are suitable for targeted drug testing

Because our approach initiates tumorigenesis by introducing defined gene aberrations, the neoCORs could potentially be used for targeted drug testing. To examine this, we assessed

Europe PMC Funders Author Manuscripts
Europe PMC Funders Author Manuscripts

Europe PMC Funders Author Manuscripts

Europe PMC Funders Author Manuscripts

the effect of the EGFR inhibitor afatinib, currently in a clinical trial for GBM (NCT number NCT02423525), as a proof of principle (Fig. 6a). Forty days after treatment, afatinib-treated samples showed significantly reduced ratios of tumor cells in GBM-1 ($P = 0.0005$) and GBM-3 ($P = 0.0004$) organoids compared with those in DMSO-treated neoCORs from the same groups (Fig. 6b,c), but no effect in the MYC^{OE} and GBM-2 groups (Fig. 6d,e), consistent with the fact that only GBM-1 and GBM-3 organoids show EGFR overactivation. Thus, neoCORs can be used to test the effect of chemical compounds on tumors that originate from specific driver mutations.

In an effort to adapt this method for large-scale screening, we modified the neoCOR system to include firefly luciferase to enable measurement of tumor size (Supplementary Fig. 9a). We applied five different EGFR inhibitors—afatinib, erlotinib, and gefitinib, which are approved for different types of cancers, and the experimental drugs canertibib and pelitinib —to GBM-1 organoids. Forty days after drug treatment, organoids treated with afatinib ($P = 0.0076$) and erlotinib ($P = 0.0074$) showed significantly reduced firefly luciferase activity in comparison with DMSO-treated neoCORs (Supplementary Fig. 9b). Thus, these results suggest that our model could be used to identify the efficacy of different compounds in the context of drug screening.

Discussion

By recapitulating genetic aberrations found in people with brain cancer via genome-editing techniques in cerebral organoids, we have generated a new in vitro model system for human brain tumors, which we have named neoCORs. These models exhibit many features of cancer, such as cellular identities, cancer-pathway-specific transcriptome profiles, and the capacity for in vivo expansion and invasion. We identified three combinations of mutations that induce glial-orientated differentiation and abnormal overgrowth, indicating their glial neoplasm-like identities. By overexpressing the oncogene *MYC*, we were able to generate neoCORs with histopathological features, cellular identities, and transcriptome signatures very similar to those described for human CNS-PNET30,40, a tumor for which no successful animal or in vitro model exists47. It is interesting to note that the amplification of *MYC* alone was sufficient to initiate CNS-PNET-like neoplasm in cerebral organoids within a very short period of time, whereas in animal models, normally additional genetic events such as the loss of *p53* and much longer experimental times are required, with low incidence27.

Unlike previous 3D culture models, such as brain tumor spheres9,48, neoCORs allow the functional analysis of genome aberrations within the same genetic background. In organoids started from patient-derived induced pluripotent stem cells, neoCORs could be further used to test the susceptibility of individuals to different combinations of driver mutations.

In contrast to brain tumor spheres and 2D glioblastoma cell cultures, neoCORs mimic in vivo structural organization, to a certain degree. They contain both tumor cells and normal cells within the same culture, so that interactions between transformed and nontransformed cells can be analyzed. This feature of neoCORs makes them not only very useful for studies of essential tumor biology, but also valuable for preclinical investigation. For drug screening,

Europe PMC Funders Author Manuscripts

Europe PMC Funders Author Manuscripts

this particular situation allows for an analysis of antitumor effects accompanied by a safety test in the same system. Like most organoid systems, neoCORs are limited by their lack of vasculature, and therefore certain features of GBM such as glomeruloid microvascular proliferations and perivascular palisading necrosis are not observable. Coculture organoid systems like the ones generated for microglia49 and/or endothelial cells50 might help scientists overcome these limitations in the future.

Taken together, our results demonstrate the power of the neoCOR model system to further knowledge of human brain tumor biology by enabling screening of tumorigenic drivers. The system will complement other models and clinical studies designed to investigate molecular mechanisms of tumor initiation, invasion, and progression. It also opens the doors to validation of potential pharmacologic and biologic therapeutic approaches and exploratory drug discovery.

Online Methods

A step-by-step protocol is available as a Supplementary Protocol and has been submitted as an open resource to the *Protocol Exchange*51.

Plasmid constructs and materials

For overexpression constructs, based on the Sleeping Beauty transposase system, the CMV promoter from pCMV(CAT)T7-SB100 (Addgene cat. no.: 34879)52 was replaced with the CAG promotor from pCAGEN (Addgene cat. no.: 11160)53. We cloned IRDR-R and IRDR-L sequences from pT2/LTR7-GFP (Addgene cat. no.: 62541)54 into pCAGEN to produce pCAG-GS/IR. cDNAs used for overexpression were amplified from human cDNA and cloned into the multiple cloning site of pCAG-GS/IR. With the help of SB transposase SB100X (pCAG-SB100X), CAG-GFP and CAG-oncogenes were integrated into the genome of cells in organoids. To introduce gene mutations, we cloned short guide RNAs of tumour suppressors into CRISPR/Cas9 vector pX330-U6-Chimeric_BB-CBh-hSpCas9 (Addgene cat. no.: 42230)55. All cloning primers are listed in the Supplementary Table 2 and 3.

Mice

MF-1 nu/nu nude mice (HsdOla:MF1-*Foxn1*^{nu}, Envigo (formerly Harlan)) were bred and maintained in the IMBA animal facility in accordance with Austrian law. All animal experiments were performed under ethical animal license protocols from the Austrian Ministry of Science, Research, and Economics (BMWFW).

Human embryonic stem cell culture

Feeder-free (FF) H9 human embryonic stem cells (hESCs) were obtained from WiCell and verified as being of normal karyotype and contamination free. FF H9 hESCs were cultured in an FF manner on Matrigel (Corning; hESC-qualified Matrix)-coated plates with mTeSR medium (Stemcell Technologies). Feeder-dependent (FD) H9 hESCs were obtained from WiCell and verified as contamination free. FD H9 hESCs were cultured on CF-1-γ-irradiated mouse embryonic stem cells (mouse embryonic fibroblasts) (GSC-6001G; Global Stem) according to WiCell protocols. All cell lines were routinely checked for mycoplasma

Europe PMC Funders Author Manuscripts

Europe PMC Funders Author Manuscripts

and tested negative. All stem cells were maintained in a 5% CO_2 incubator at 37 °C. Standard procedures were used to culture and split hESCs as explained previously17. All hESCs were authenticated with an Infinium PsychArray-24 kit (Illumina).

Generation of cerebral organoids

Cerebral organoids were cultured as previously described17. Briefly, for the generation of EBs, hESCs were trypsinized into single cells, and 9,000 cells were plated into each well of an ultra-low-binding 96-well plate (Corning) in human ES medium containing low-concentration basic fibroblast growth factor (4 ng/ml) and 50 μM Rho-associated protein kinase (ROCK) inhibitor (Calbiochem). EBs were fed every 3 d for 6 d and then transferred to neural induction media to form neuroepithelial tissues. After 5–7 d in neural induction medium, EBs were embedded in droplets of Matrigel (Corning) and cultured in differentiation medium without vitamin A. Finally, the EB droplets were transferred to a 10-cm dish containing differentiation medium with vitamin A and cultured on an orbital shaker. Media were changed weekly.

Nucleofection of organoids to induce gene mutation/amplification

To initiate brain tumors, we introduced tumor-suppressor mutations and/or oncogene amplifications into neuroepithelial cells at the end of neural induction culture, right before Matrigel embedding. Briefly, 10–15 EBs were collected, resuspended in nucleofection reagent (Nucleofector kits for human stem cells; Lonza) containing plasmids, and transferred into nucleofection vials. Nucleofection was carried out according to the manufacturer's protocol. After electroporation, EBs were carefully transferred to a 6-cm dish containing neural induction medium and cultured at 37 °C in an incubator for 4 h. Then nucleofected EBs were embedded in Matrigel and cultured for organoids as described. The neoCORs with significant overgrowth of GFP^+ cells were selected for further investigations, in which the samples were randomly allocated.

Adherent cell culture of dissociated embryoid bodies.

One day after nucleofection, the EBs were trypsinized at 37 °C for 20 min to make a single-cell suspension. Then cells were plated on poly-D-lysine- and laminin-coated coverslips in neural induction medium with ROCK inhibitor, and cultured in a 5% CO_2 incubator at 37 °C. Further immunofluorescence staining and analysis were carried out the next day.

RNA-sequencing and analysis

Organoids from control and neoplastic groups were collected 40 d and 4 months after nucleofection, and trypsinized with shaking at 37 °C for 30 min. GFP^+ cells were sorted according to the example gating strategy (Supplementary Fig. 10), and total RNA was isolated with an RNeasy micro kit (Qiagen) according to the manufacturer's instructions. RNA concentration and quality were analyzed with an RNA 6000 Nano Chip (Agilent Technologies). Messenger RNA (mRNA) was enriched with the SMART-Seq v4 ultra-low-input RNA kit (TaKaRa) according to the manufacturer's protocol. Libraries were prepared with the NEB Next Ultra Directional RNA library prep kit for Illumina (NEB). Barcoded samples were multiplexed and sequenced 50 bp single-end on a HighSeq 2500 (Illumina).

Europe PMC Funders Author Manuscripts

Europe PMC Funders Author Manuscripts

mRNA sample isolation, library preparation, and sequencing were done at the VBCF NGS Unit (https://www.vbcf.ac.at).

The unstranded reads were screened for ribosomal RNA by alignment with BWA (v0.7.12) against known rRNA sequences (RefSeq). The rRNA subtracted reads were aligned with TopHat (v2.1.1) against the *Homo sapiens* genome (hg38). Microexon search was enabled. Additionally, a gene model was provided as GTF (UCSC, 2015_01, hg38). rRNA loci were masked on the genome for downstream analysis. Aligned reads were subjected to TPM estimation with Kallisto (v0.43.0). Furthermore, the aligned reads were counted with HTSeq (v0.6.1; intersection-nonempty) and the genes were subjected to differential expression analysis with DESeq2 (v1.12.4).

Before the bioinformatics analysis, the expression of oncogenes according to the genome-editing manipulation was checked, and one 4-month-old sample from the GBM-3 neoCOR group was excluded from further analysis because of the failure to introduce overexpression of EGFRvIII.

Principal component analysis was carried out with the top 500 variable genes between normal cells from CTRL organoids and tumor cells from different neoCOR groups. A Venn diagram hypergeometric test was conducted on genes with differential expression between cluster 2 or cluster 3 and the CTRL, and KEGG pathway enrichment analysis was carried out on genes with differential expression between cluster 2 and cluster 3 with an adjusted absolute $\log_2$(fold change (FC)) value > 0.5 and adjusted *P* value < 0.05. A Venn diagram hypergeometric test was performed in R language. KEGG pathway enrichment was analyzed with DAVID Bioinformatics (https://david.ncifcrf.gov)56. The heat map of RNA-seq data was generated with MeV57. For the heat map of tumor-type gene profiling (Fig. 3c), genes that were differentially expressed between cluster 2 and cluster 3 (adjusted absolute $\log_2$FC value > 1 or < –1 and adjusted *P* value < 0.05) were selected from the list of differentially expressed genes (adjusted absolute $\log_2$FC value > 1 or < –1 and adjusted *P* value < 0.05) from human primary tumor transcriptome analysis30. For the heat map of hierarchical clustering analysis of GBM invasiveness-relevant genes (Fig. 5e), we selected genes from any individual GBM groups with differential expression relative to that in CTRL organoids with an adjusted absolute $\log_2$FC value > 0.5 and adjusted *P* value < 0.05. The heat map was created from $\log_2$(TPM) transformed data that were row (gene) normalized using the “Median Center Genes/Rows” and “Normalize Genes/Rows” functions to report data as relative expression between samples.

Verification of genome alteration introduced by SB and CRISPR-Cas9

To test whether the genome-editing techniques actually altered the genome in tumor cells, we used FACS to sort GFP^+ tumor cells for genomic DNA isolation for genotyping and for RNAs to verify the expression of oncogenes. RNAs were isolated with the RNeasy micro kit (Qiagen), and cDNA was synthesized according to a previously described method58. RT-PCR for MYC, EGFR/EGFRvIII, and TBP was done with the primers listed in Supplementary Table 4. Genomic DNAs were isolated with DNeasy Blood & Tissue kits (Qiagen) according to the manufacturer’s instruction. The CRISPR–Cas9-targeted genome loci of tumor-suppressor genes were amplified using the primers listed in Supplementary

Europe PMC Funders Author Manuscripts

Europe PMC Funders Author Manuscripts

Table 5. The PCR products were inserted into T vector (Promega) according to the manufacturer's instructions. Ninety-six colonies per gene were cultured for sequencing.

Renal subcapsular engrafting

All procedures were performed in accordance with institutional animal care guidelines and ethical license protocols. Briefly, adult MF1 nu/nu male mice (8–12 weeks old) were anesthetized with ketamine solution. After disinfection of the surgical site with 70% alcohol, a 1.5- to 2-cm incision was made and the kidney was carefully exteriorized. A 2- to 4-mm incision was made in the renal capsule with a pipette tip, and a capsule pocket for the grafts was made with a blunted glass Pasteur pipette. Two-month-old organoids from each group were carefully implanted under renal capsules (one organoid per capsule). Then the kidney was gently replaced in the retroperitoneal cavity. During the exteriorization, the kidney was kept hydrated by application of PBS with penicillin–streptomycin. The kidneys were collected 1 week and 1.5 months after xenograft for further analysis. The experiments were performed three times independently with different numbers of mice/grafts. In total, at least three engrafted organoids per group were analyzed.

Immunofluorescence and immunohistochemistry

For immunofluorescence staining, tissues were fixed in 4% paraformaldehyde (PFA) at 4 °C overnight. The tissues were dehydrated in 30% sucrose overnight, embedded in Tissue-Tek (VWR), and then cryosectioned at 16 μm. Sections were blocked and permeabilized in 0.5% Triton X-100 and 4% normal donkey serum (NDS) in PBS at room temperature (RT). Sections were incubated at 4 °C with primary antibody in 0.1% Triton X-100 and 4% NDS in PBS. After being washed three times for 10 min with PBS, sections were incubated with secondary antibodies in 0.1% Triton X-100 and 4% NDS in PBS and DAPI consecutively for visualization of the immunostains. For immunofluorescence staining of adherent cell culture, cells on a coverslip were fixed in 4% PFA for 30 min, blocked and permeabilized in 0.5% Triton X-100 and 4% NDS in PBS at RT for 30 min, and incubated with primary and secondary antibodies for 1 h at RT sequentially. Then the cells were incubated with DAPI for nuclei staining and mounted with DAKO fluorescence mounting medium. The primary and secondary antibodies used for immunofluorescence are listed in Supplementary Tables 6 and 7. Images were captured with a confocal microscope (Zeiss LSM 780) and a fluorescence microscope (Zeiss Axio Imager 2). Quantification of images from three independent preparations of neoCORs was done in Fiji. The experiments were performed on samples from three independent preparations.

For histologic and immunohistochemical staining, tissues were fixed in 4% paraformaldehyde overnight. Fixed tissues were rinsed in PBS, dehydrated by immersion in an ascending ethanol gradient (70%, 90%, and 100% ethanol), embedded in paraffin, and sectioned at a thickness of 2–5 μm. Sections were stained via a routine hematoxylin and eosin (H&E) protocol in a Microm HMS 740 automated stainer. Immunohistochemistry was performed with the Leica Bond III automated immunostainer. The primary and secondary antibodies used in this study are listed in Supplementary Tables 6 and 7. Slides were reviewed with a Zeiss Axioskop 2 MOT microscope, and images were acquired with a SPOT Insight digital camera. Slides were also scanned with a Pannoramic 250 Flash II scanner (3D

Europe PMC Funders Author Manuscripts

Europe PMC Funders Author Manuscripts

Histech). Digital slides were reviewed and images acquired with the Pannoramic Viewer software (3D Histech). Slides were reviewed by a board-certified veterinary comparative pathologist (A.K.).

For quantification of immunofluorescence staining, images from at least three organoids per group, collected from three independent experiments, were analyzed. Detailed sample sizes are stated in the relevant figure legends and the associated source data (available online).

Drug testing on neoplastic cerebral organoids

For drug testing, neoCORs were first grown for 2 months and then subjected to drug treatment for 40 d. EGFR inhibitors afatinib (http://www.selleckchem.com; cat. no. S1011), erlotinib (http://www.selleckchem.com; cat. no. S7786), gefitinib (http://www.selleckchem.com; cat. no. S1025), canertinib (http://www.selleckchem.com; cat. no. S1019), and pelitinib (Sigma-Aldrich; cat. no. 257933-82-7) (final concentration: 1 μM) were applied, and DMSO was used as the control. After drug treatment, neoCORs were trypsinized for single-cell preparation and then subjected to FACS analysis. We counted total cell numbers to evaluate the cytotoxicity of the drugs. The drug-testing experiments were performed twice independently.

Flow cytometry

Flow cytometry experiments differed according to the different experimental purposes. For RNA-seq analysis, organoids were trypsinized to make single-cell suspensions. GFP^+ cells were collected with a BD FACSAria III. Live cells were gated to sort GFP^+ cells for further RNA-seq analysis. For drug-testing experiments, organoids were trypsinized to make single-cell suspensions. The proportion of GFP^+ cells was analyzed with a BD LSR Fortessa 2. Live cells were gated for analysis of the GFP^+ cell proportion. All cells were analyzed for GFP^+cell proportion. Data were analyzed with BD FACSDiva software. An example representing the gating strategy is presented in Supplementary Fig. 10.

Statistical Analysis

Statistical analysis was carried out with GraphPad Prism 7. Statistical analysis of quantification was done by unpaired two-tailed Student's *t*-test for comparison of two groups, and by one-way ANOVA with Tukey's test or Dunnett's multiple comparisons test for comparisons of multiple groups. The threshold for statistical significance was $P < 0.05$. No statistical method was used to predetermine the sample size. Sample sizes for experiments were estimated on the basis of previous experience with a similar setup that showed significance. Experiments were not randomized and were not blindly analyzed. All details on sample size, statistical analysis, mean ± s.d., and adjusted *P* value for each experiment are provided in the relevant figure legends and in the associated source data (available online).

Supplementary Material

Refer to Web version on PubMed Central for supplementary material.

Europe PMC Funders Author Manuscripts

Europe PMC Funders Author Manuscripts

Acknowledgements

We are grateful to all members of the Knoblich laboratory for discussions, and H. Gustafson and S. Wolfinger for technical support. We thank O. Wüseke and F. Bonnay for the comments on the manuscript. We thank T. Müller, P. Pasierbek, G. Petri, M. Weninger, G. Schmauss, and T. Lendl for FACS and help with imaging. We thank A. Piszczek, T. Engelmaier, J. Klughofer, and and M. Zeba for tissue processing and immunohistochemical staining. We thank the Next Generation Sequencing Facility for Next Generation sequencing. We thank Boehringer Ingelheim RCV GmbH & Co KG for providing EGFR inhibitors. We thank W. Hu for statistical advice. J.A. Bagley received funding from an EMBO postdoctoral fellowship, and funding from European Union's Horizon 2020 research and innovation programme under the Marie Skłodowska-Curie grant agreement (No.707109). Work in J.A. Knoblich laboratory is supported by the Austrian Academy of Sciences, the Austrian Science Fund (Z_153_B09), and an advanced grant from the European Research Council (ERC).

References

1. Ostrom QT, et al. CBTRUS Statistical Report: Primary Brain and Other Central Nervous System Tumors Diagnosed in the United States in 2009-2013. Neuro-oncology. 2016; 18:v1–v75. [PubMed: 28475809]
2. Lui JH, Hansen DV, Kriegstein AR. Development and evolution of the human neocortex. Cell. 2011; 146:18–36. [PubMed: 21729779]
3. McLendon R, et al. Comprehensive genomic characterization defines human glioblastoma genes and core pathways. Nature. 2008; 455:1061–1068. [PubMed: 18772890]
4. Brennan CW, et al. The somatic genomic landscape of glioblastoma. Cell. 2013; 155:462–477. [PubMed: 24120142]
5. Parsons DW, et al. The Genetic Landscape of the Childhood Cancer Medulloblastoma. Science. 2011; 331:435–439. [PubMed: 21163964]
6. Huszthy PC, et al. In vivo models of primary brain tumors: pitfalls and perspectives. Neuro-oncology. 2012; 14:979–993. [PubMed: 22679124]
7. Hu B, et al. Epigenetic Activation of WNT5A Drives Glioblastoma Stem Cell Differentiation and Invasive Growth. Cell. 2016; 167:1281–1295.e18. [PubMed: 27863244]
8. Singh SK, et al. Identification of human brain tumour initiating cells. Nature. 2004; 432:396–401. [PubMed: 15549107]
9. Hubert CG, et al. A three-dimensional organoid culture system derived from human glioblastomas recapitulates the hypoxic gradients and cancer stem cell heterogeneity of tumors found in vivo. Cancer Research. 2016; doi: 10.1158/0008-5472.CAN-15-2402
10. Zhu Z, et al. Zika virus has oncolytic activity against glioblastoma stem cells. J Exp Med. 2017; 214:2843–2857. [PubMed: 28874392]
11. Sato T, et al. Single Lgr5 stem cells build crypt-villus structures in vitro without a mesenchymal niche. Nature. 2009; 459:262–265. [PubMed: 19329995]
12. Kelava I, Lancaster MA. Stem Cell Models of Human Brain Development. Cell Stem Cell. 2016; 18:736–748. [PubMed: 27257762]
13. Clevers H, Loh KM, Nusse R. An integral program for tissue renewal and regeneration: Wnt signaling and stem cell control. Science. 2014; 346:1248012–1248012. [PubMed: 25278615]
14. Lancaster MA, Knoblich JA. Organogenesis in a dish: Modeling development and disease using organoid technologies. Science. 2014; 345:1247125–1247125. [PubMed: 25035496]
15. Johnson JZ, Hockemeyer D. Human stem cell-based disease modeling: prospects and challenges. Curr Opin Cell Biol. 2015; 37:84–90. [PubMed: 26546888]
16. Neal JT, Kuo CJ. Organoids as Models for Neoplastic Transformation. Annu Rev Pathol Mech Dis. 2016; 11:199–220.
17. Lancaster MA, et al. Cerebral organoids model human brain development and microcephaly. Nature. 2013; 501:373–379. [PubMed: 23995685]
18. Bershteyn M, et al. Human iPSC-Derived Cerebral Organoids Model Cellular Features of Lissencephaly and Reveal Prolonged Mitosis of Outer Radial Glia. Cell Stem Cell. 2017; :1–29. DOI: 10.1016/j.stem.2016.12.007

Europe PMC Funders Author Manuscripts

Europe PMC Funders Author Manuscripts

19. Mariani J, et al. FOXG1-Dependent Dysregulation of GABA/ Glutamate Neuron Differentiation in Autism Spectrum Disorders. Cell. 2015; 162:375–390. [PubMed: 26186191]
20. Iefremova V, et al. An Organoid-Based Model of Cortical Development Identifies Non-Cell-Autonomous Defects in Wnt Signaling Contributing to Miller-Dieker Syndrome. Cell Rep. 2017; 19:50–59. [PubMed: 28380362]
21. Louis DN, et al. The 2016 World Health Organization Classification of Tumors of the Central Nervous System: a summary. Acta Neuropathol. 2016; 131:803–820. [PubMed: 27157931]
22. Zhu Y, et al. Early inactivation of p53 tumor suppressor gene cooperating with NF1 loss induces malignant astrocytoma. Cancer Cell. 2005; 8:119–130. [PubMed: 16098465]
23. Kwon C-H, et al. Pten Haploinsufficiency Accelerates Formation of High-Grade Astrocytomas. Cancer Research. 2008; 68:3286–3294. [PubMed: 18451155]
24. Zheng H, et al. p53 and Pten control neural and glioma stem/progenitor cell renewal and differentiation. Nature. 2008; 455:1129–1133. [PubMed: 18948956]
25. Marino S, Vooijs M, van Der Gulden H, Jonkers J, Berns A. Induction of medulloblastomas in p53-null mutant mice by somatic inactivation of Rb in the external granular layer cells of the cerebellum. Genes & Development. 2000; 14:994–1004. [PubMed: 10783170]
26. Gibson P, et al. Subtypes of medulloblastoma have distinct developmental origins. Nature. 2010; 468:1095–1099. [PubMed: 21150899]
27. Momota H, Shih AH, Edgar MA, Holland EC. c-Myc and beta-catenin cooperate with loss of p53 to generate multiple members of the primitive neuroectodermal tumor family in mice. Oncogene. 2008; 27:4392–4401. [PubMed: 18372915]
28. Han Z-Y, et al. The occurrence of intracranial rhabdoid tumours in mice depends on temporal control of Smarcb1 inactivation. Nature Communications. 2016; 7:10421.
29. Chen J, McKay RM, Parada LF. Malignant glioma: lessons from genomics, mouse models, and stem cells. Cell. 2012; 149:36–47. [PubMed: 22464322]
30. Sturm D, et al. New Brain Tumor Entities Emerge from Molecular Classification of CNS-PNETs. Cell. 2016; 164:1060–1072. [PubMed: 26919435]
31. Biegel JA, et al. Germ-line and acquired mutations of INI1 in atypical teratoid and rhabdoid tumors. Cancer Research. 1999; 59:74–79. [PubMed: 9892189]
32. Rogers HA, et al. WNT/β-catenin pathway activation in Myc immortalised cerebellar progenitor cells inhibits neuronal differentiation and generates tumours resembling medulloblastoma. British Journal of Cancer. 2012; 107:1144–1152. [PubMed: 22929883]
33. Hutter S, Bolin S, Weishaupt H, Swartling F. Modeling and Targeting MYC Genes in Childhood Brain Tumors. Genes. 2017; 8:107–19.
34. Atkins M, et al. An Ectopic Network of Transcription Factors Regulated by Hippo Signaling Drives Growth and Invasion of a Malignant Tumor Model. Curr Biol. 2016; 26:2101–2113. [PubMed: 27476594]
35. Gutmann DH, Saporito-Irwin S, DeClue JE, Wienecke R, Guha A. Alterations in the rap1 signaling pathway are common in human gliomas. Oncogene. 1997; 15:1611–1616. [PubMed: 9380414]
36. Clark PA, et al. Activation of Multiple ERBB Family Receptors Mediates Glioblastoma Cancer Stem-like Cell Resistance to EGFR-Targeted Inhibition. NEO. 2012; 14:420–IN13.
37. Mayer A, Schneider F, Vaupel P, Sommer C, Schmidberger H. Differential expression of HIF-1 in glioblastoma multiforme and anaplastic astrocytoma. Int J Oncol. 2012; 41:1260–1270. [PubMed: 22825389]
38. Puliyappadamba VT, Hatanpaa KJ, Chakraborty S, Habib AA. The role of NF-κB in the pathogenesis of glioma. Mol Cell Oncol. 2014; 1:e963478. [PubMed: 27308348]
39. Tavares CB, et al. Expression of estrogen and progesterone receptors in astrocytomas: a literature review. Clinics (Sao Paulo). 2016; 71:481–486. [PubMed: 27626480]
40. Ellison, D, , et al. Neuropathology. Elsevier Health Sciences; 2012.
41. Rocchi A, et al. CD99 inhibits neural differentiation of human Ewing sarcoma cells and thereby contributes to oncogenesis. J Clin Invest. 2010; 120:668–680. [PubMed: 20197622]

Europe PMC Funders Author Manuscripts

42. Schmitz M, et al. Identification of SOX2 as a novel glioma-associated antigen and potential target for T cell-based immunotherapy. British Journal of Cancer. 2007; 96:1293–1301. [PubMed: 17375044]
43. Seol HJ, et al. Overexpression of CD99 Increases the Migration and Invasiveness of Human Malignant Glioma Cells. Genes & Cancer. 2012; 3:535–549. [PubMed: 23486730]
44. Iwadate Y. Epithelial-mesenchymal transition in glioblastoma progression. Oncol Lett. 2016; 11:1615–1620. [PubMed: 26998052]
45. Binder DK, Berger MS. Proteases and the biology of glioma invasion. J Neurooncol. 2002; 56:149–158. [PubMed: 11995816]
46. Paw I, Carpenter RC, Watabe K, Debinski W, Lo H-W. Mechanisms regulating glioma invasion. Cancer Lett. 2015; 362:1–7. [PubMed: 25796440]
47. Trojanowski JQ, et al. In vivo and in vitro models of medulloblastomas and other primitive neuroectodermal brain tumors of childhood. Mol Chem Neuropathol. 1994; 21:219–239. [PubMed: 8086035]
48. Grotzer MA, Neve A, Baumgartner M. Dissecting brain tumor growth and metastasis in vitro and ex vivo. JCMT. 2016; 2:149–14.
49. Muffat J, et al. Efficient derivation of microglia-like cells from human pluripotent stem cells. Nat Med. 2016; 22:1358–1367. [PubMed: 27668937]
50. Cui X, et al. Hacking macrophage-associated immunosuppression for regulating glioblastoma angiogenesis. Biomaterials. 2018; 161:164–178. [PubMed: 29421553]
51. Bian S, Knoblich JA. Genetic engineering to initiate tumorigenesis in cerebral organoids. Protocol Exchange.
52. Mátés L, et al. Molecular evolution of a novel hyperactive Sleeping Beauty transposase enables robust stable gene transfer in vertebrates. Nat Genet. 2009; 41:753–761. [PubMed: 19412179]
53. Matsuda T, Cepko CL. Electroporation and RNA interference in the rodent retina in vivo and in vitro. Proc Natl Acad Sci USA. 2004; 101:16–22. [PubMed: 14603031]
54. Wang J, et al. Primate-specific endogenous retrovirus-driven transcription defines naive-like stem cells. Nature. 2014; 516:405–409. [PubMed: 25317556]
55. Ran FA, et al. Genome engineering using the CRISPR-Cas9 system. Nat Protoc. 2013; 8:2281–2308. [PubMed: 24157548]
56. Huang DW, Sherman BT, Lempicki RA. Systematic and integrative analysis of large gene lists using DAVID bioinformatics resources. Nat Protoc. 2009; 4:44–57. [PubMed: 19131956]
57. Saeed AI, et al. TM4: a free, open-source system for microarray data management and analysis. BioTechniques. 2003; 34:374–378. [PubMed: 12613259]
58. Bagley JA, Reumann D, Bian S, Lévi-Strauss J, Knoblich JA. Fused cerebral organoids model interactions between brain regions. Nature Methods. 2017; 14:743–751. [PubMed: 28504681]

Europe PMC Funders Author Manuscripts

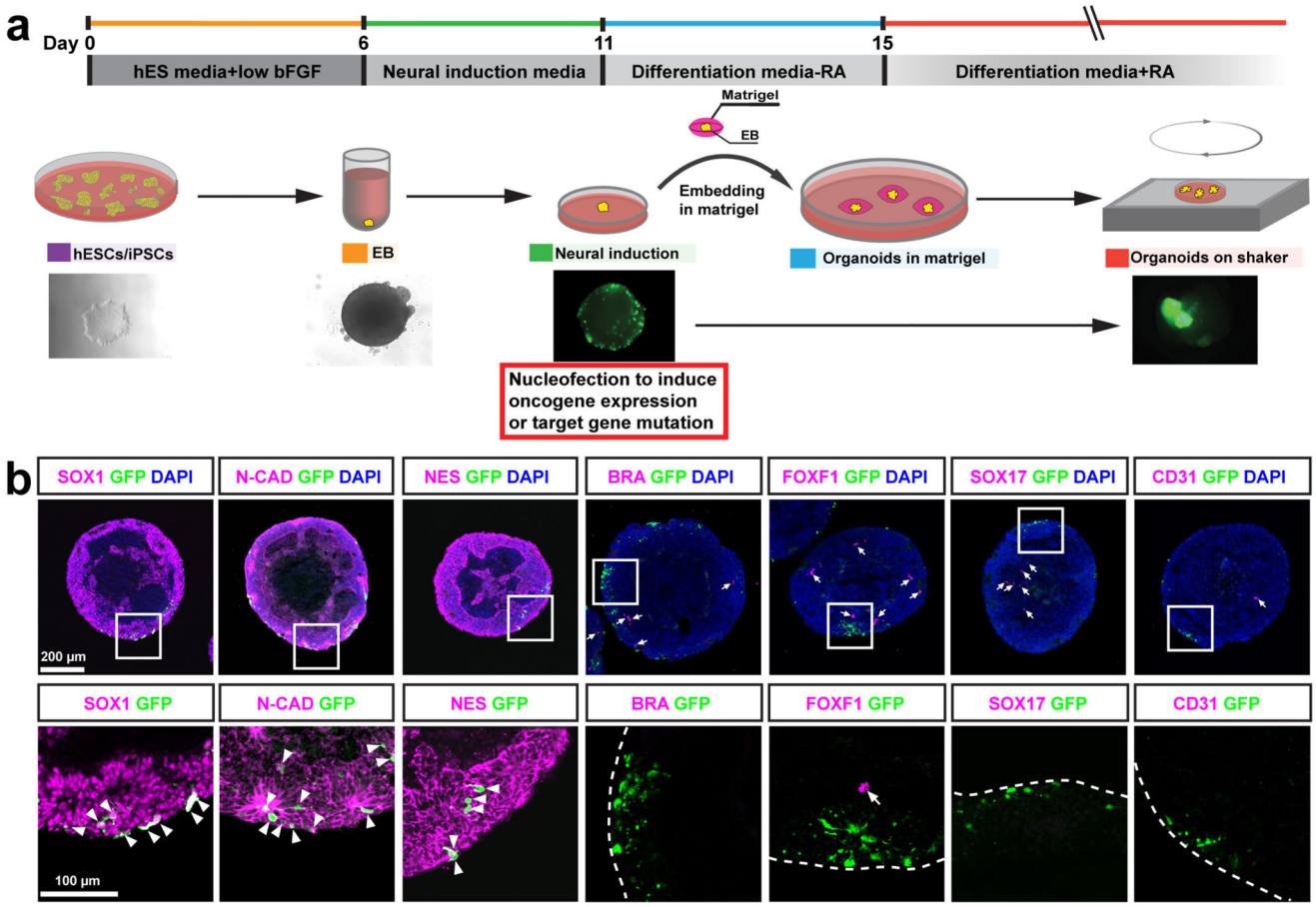

Figure 1. Introducing genome-editing constructs into neural stem/precursor cells of cerebral organoids.

a, Schematic of cerebral organoid culture and nucleofection strategy. EB, embryoid body; bFGF, basic fibroblast growth factor; hESCs, human embryonic stem cells; iPSCs, induced pluripotent stem cells; RA, retinoic acid. **b**, Immunofluorescence staining for the indicated markers in EBs 1 d after nucleofection. The images in the bottom row are high-magnification views of nucleofected cells (magnified regions are those outlined by white squares in the images above). Arrowheads point to nucleofected cells (GFP) that express NS/PC markers; arrows point to cells expressing mesodermal (BRA or FOXF1) or endodermal (SOX17 or CD31) markers. Dashed lines indicate the boundaries of EBs. This experiment was performed twice independently, with same results obtained each time. N-CAD, N-cadherin; NES, Nestin; BRA, brachyury. Scale bars, 200 μm (upper panel) or 100 μm (lower panel).

Europe PMC Funders Author Manuscripts
Europe PMC Funders Author Manuscripts

Europe PMC Funders Author Manuscripts

Europe PMC Funders Author Manuscripts

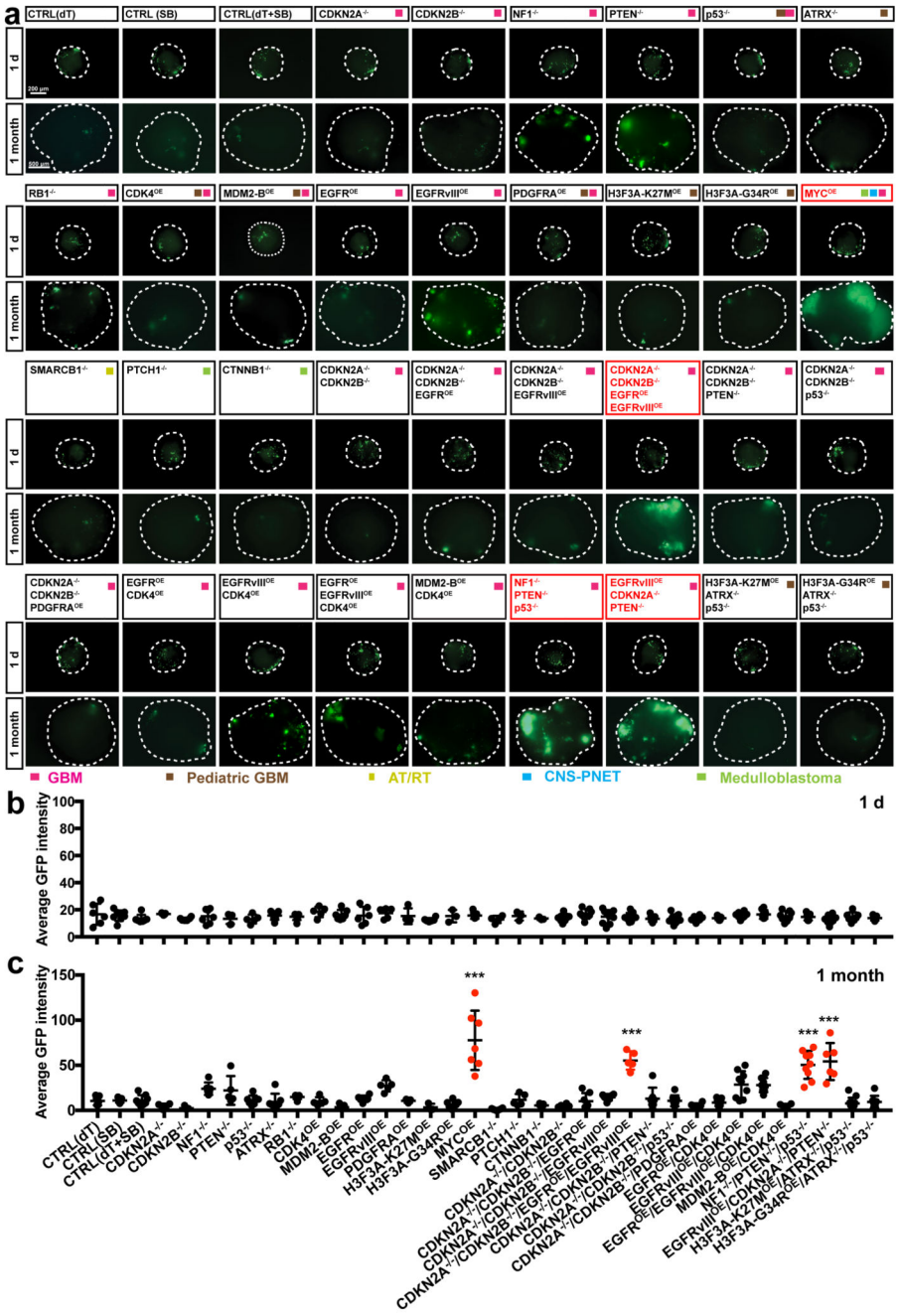

Figure 2. Clonal mutagenesis in organoids induces tumour overgrowth.

a–**c**, Immunofluorescence images (**a**) and quantification of the GFP fluorescence intensity (**b**,**c**) of organoids mutagenized with the indicated mutation combinations 1 d (**b**) and 1 month (**c**) after nucleofection. Organoids from four groups showed significant overgrowth at 1 month: MYC^{OE} ($n = 7$; adjusted $P < 0.0001$ versus CTRL(SB)), *CDKN2A*$^{-/-}$/*CDKN2B*$^{-/-}$/*EGFR*^{OE}/*EGFRvIII*^{OE} ($n = 5$; adjusted $P < 0.0001$ versus CTRL (dT + SB)), *NF1*$^{-/-}$/*PTEN*$^{-/-}$/*p53*$^{-/-}$ ($n = 9$; adjusted $P < 0.0001$ versus CTRL(dT + SB)), and *EGFRvIII*^{OE}/*PTEN*$^{-/-}$/*CDKN2A*$^{-/-}$ ($n = 6$; adjusted $P < 0.0001$ versus CTRL(dT + SB)).

This experiment was performed once. Statistical analysis consisted of one-way ANOVA with Tukey's test. Data are presented as mean ± s.d.; full details including all sample sizes are provided online as source data. ***$P < 0.001$. **a**, Scale bars, 200 μm (1 d) or 500 μm (1 month). AT/RT, atypical teratoid/rhabdoid tumor; dT, dTomato guide RNA.

Europe PMC Funders Author Manuscripts

Europe PMC Funders Author Manuscripts

Europe PMC Funders Author Manuscripts

Europe PMC Funders Author Manuscripts

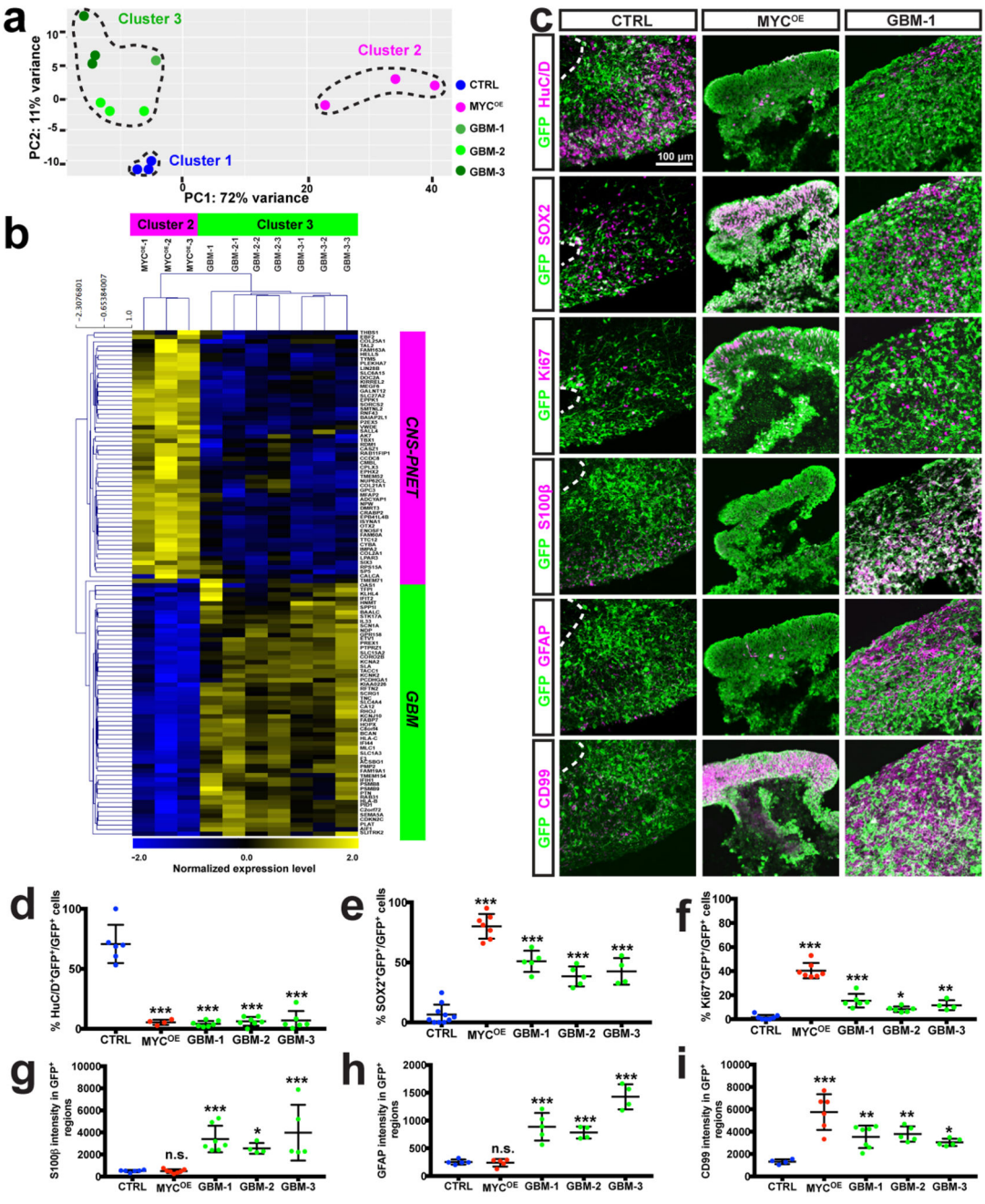

Figure 3. MYC^{OE} and GBM-like neoCORs have distinct transcriptional profiles and cellular identities.

a, Principal component (PC) analysis of the top 500 variable genes between normal cells from CTRL organoids and tumor cells from different neoCOR groups. **b**, A heat map showing normalized expression levels for genes with differential expression (adjusted absolute $\log_2$(fold change) > 1 or < –1 and adjusted *P* value < 0.05) between cluster 2 and cluster 3 ($n = 3$ for cluster 2 and $n = 7$ for cluster 3 from one experiment), selected from genes with differential expression between human primary CNS-PNET and GBM tumors.

Europe PMC Funders Author Manuscripts

Europe PMC Funders Author Manuscripts

The heat map was created from $\log_2$(TPM) (TPM: transcripts per million) transformed data that were row (gene) normalized with the “Median Center Genes/Rows” and “Normalize Genes/Rows” functions to report data as relative expression between samples. **c**, Representative immunofluorescence images of 4-month-old organoids from CTRL, MYC^{OE}, and GBM-1 groups. The staining was performed in six independent experiments, with similar results obtained each time. Scale bar, 100 μm. **d**–**i**, Quantification of the percentage of $HuC/D^+GFP^+/GFP^+$ (**d**), $SOX2^+GFP^+/GFP^+$ (**e**), and $Ki67^+GFP^+/GFP^+$ (**f**) cells, and of the intensity of S100β (**g**), GFAP (**h**), and CD99 (**i**) in different samples. Markers measured in cells shown in **c** (magenta) and Supplementary Fig. 5 for CTRL and all neoCOR groups. The staining was performed in six independent experiments, with similar results obtained each time. Quantification was performed on organoids from three independent experiments. Statistical analysis was done by one-way ANOVA with Dunnett’s test. Data are presented as mean ± s.d., and details of sample sizes and values, as well as adjusted *P* values, are available online as source data. $*P < 0.05$, $**P < 0.01$, $***P < 0.001$.

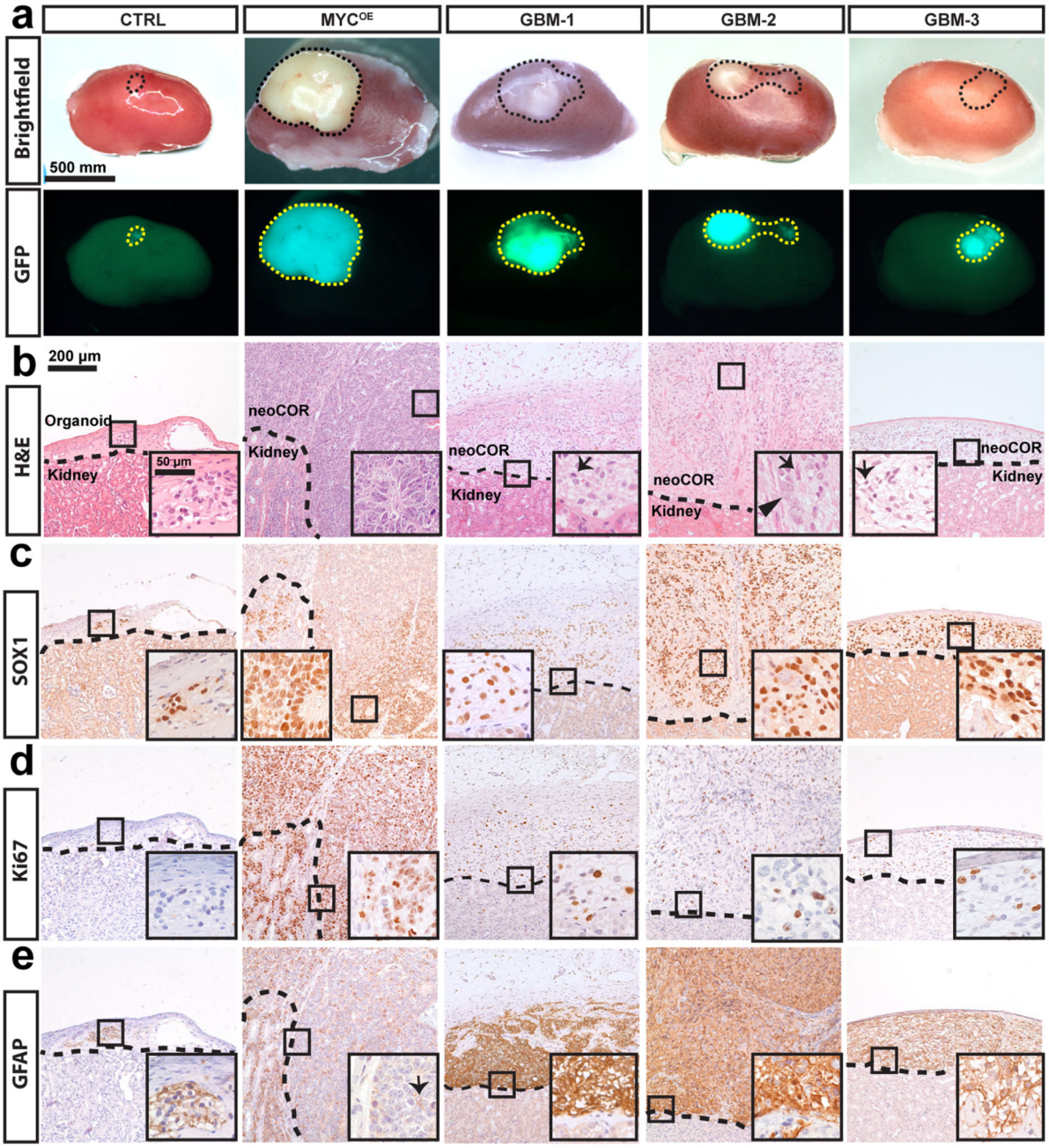

Figure 4. NeoCORs expand in renal subcapsular xenografts.

a, Bright-field and immunofluorescence images of the indicated renal subcapsular implants 1.5 months after implantation. **b**, Hematoxylin and eosin (H&E) staining of neoCORs under the renal capsule. Arrows indicate glial cells; arrowhead indicates a neuron. **c**–**e**, Immunohistochemical staining of SOX1 (**c**), Ki67 (**d**), and GFAP (**e**) in implanted organoids. Scale bars, 500 mm (**a**), 200 μm (**b**–**f**) or 50 μm (insets in **b**–**f**).

Europe PMC Funders Author Manuscripts
Europe PMC Funders Author Manuscripts

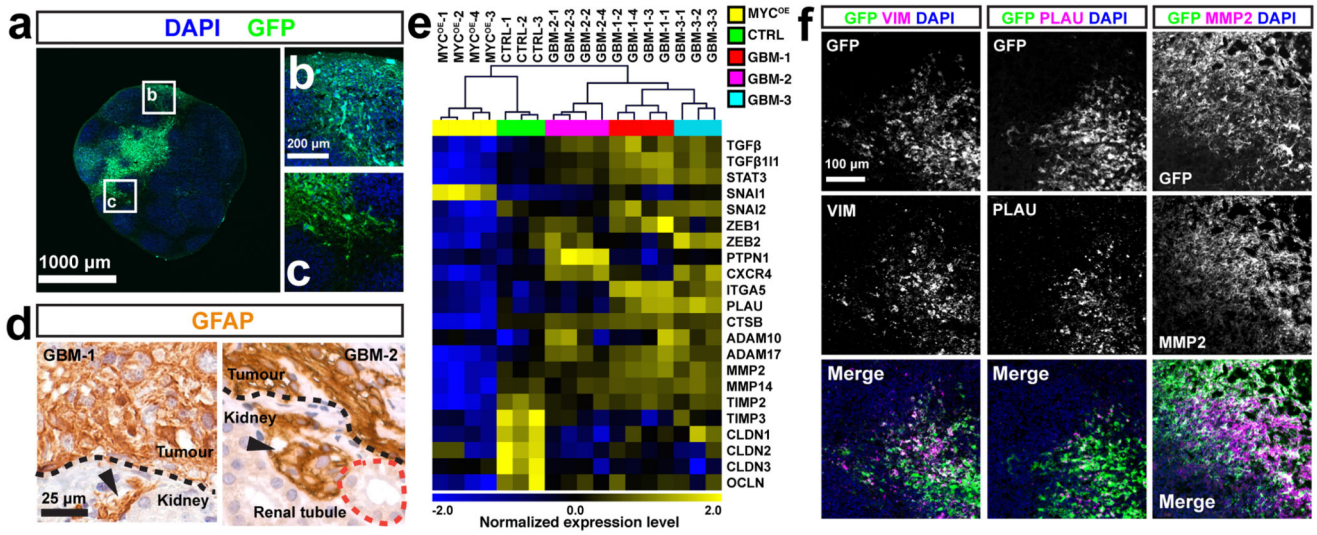

Figure 5. GBM neoCORs exhibit features of GBM invasion.

a–**c**, Representative image of the tumor–normal interface in GBM-1 neoCORs (**a**), with higher-magnification views of highlighted regions (**b**,**c**). Images are representative of at least three independent experiments. **d**, Immunohistochemical staining of GFAP in GBM-like neoCORs. Images are representative of two independent renal implantations. Dashed black lines indicate the boundary between implanted neoCORs and mouse kidney; dashed red line indicates the renal tubule. Arrowheads indicate invaded tumor cells. **e**, Hierarchical clustering analysis of GBM invasiveness-relevant genes from 4-month-old organoids ($n = 3$ CTRL organoids; $n = 4$ (MYC^{OE}, GBM-1, and GBM-2) or 3 (GBM-3) neoCORs, from three independent cultures for each group). The heat map was created from $\log_2$(TPM) transformed data that were row (gene) normalized using the “Median Center Genes/Rows” and “Normalize Genes/Rows” functions to report data as relative expression between samples. **f**, Representative immunofluorescence staining of neoCORs from the GBM-1 group for the indicated mesenchymal markers and invasiveness-relevant proteases; GFP is also shown. Images are representative of two independent experiments. Scale bars, 1,000 µm (**a**), 200 µm (**b**,**c**), 25 µm (**d**), or 100 µm (**f**).

Europe PMC Funders Author Manuscripts
Europe PMC Funders Author Manuscripts

Europe PMC Funders Author Manuscripts

Europe PMC Funders Author Manuscripts

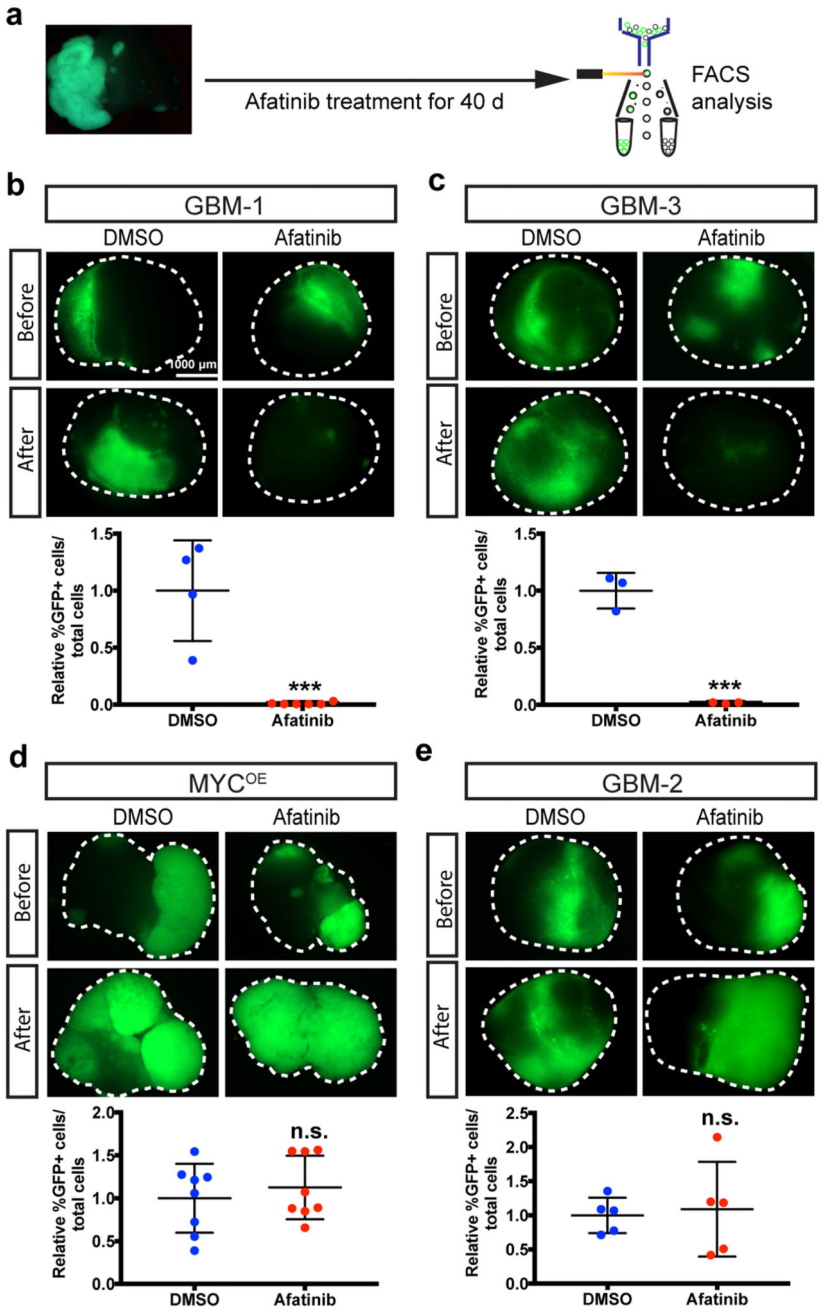

Figure 6. NeoCORs are suitable for preclinical investigations.

a, Schematic of the drug treatment and FACS analysis using neoCORs. **b**–**e**, Images and FACS quantification of cells from neoCORs after the indicated treatments. The percentage of GFP^+ cells from drug-treated groups was normalized to the percentage of GFP^+ cells from DMSO-treated neoCORs. Afatinib decreased the ratio of tumor cells in GBM-1 (**b**; $n = 6$ from one experiment; $P = 0.0005$) and GBM-3 (**c**; $n = 3$ from one experiment; $P = 0.0004$) neoCORs, but not in MYC^{OE} (**d**; $n = 8$ from one experiment; $P = 0.5261$) and GBM-2 (**e**; $n = 5$ from one experiment; $P = 0.7916$) groups. The experiments were performed twice

independently, with similar results. Statistical analysis was done by unpaired two-tailed Student's *t*-test. Data are presented as mean ± s.d.; details of sample size and values are provided online as source data. ***$P < 0.001$. Scale bar, 1,000 μm (**b**–**e**).

Europe PMC Funders Author Manuscripts

Europe PMC Funders Author Manuscripts